2018 IEEE-RAS 18th International Conference on Humanoid Robots (Humanoids)
Beijing, China, November 6-9, 2018

Compliant Biped Locomotion of Hydra, an Electro-Hydrostatically Driven Humanoid

Tianyi Ko, Ko Yamamoto, Kazuya Murotani and Yoshihiko Nakamura[1]

***Abstract*— The backdrivability of joints is a critical requirement for the robots that perform tasks in uncertain environments. While series elastic actuators are intrinsically backdrivable, their control bandwidth is limited by the low resonant frequency of the elastic component. To simultaneously realize both of the backdrivability and high control bandwidth, Electro-Hydrostatic Actuator (EHA) is a solution. Based on this idea, we developed the fully electro-hydrostatically driven humanoid robot Hydra, while its evaluation was limited to the joint level one. In this paper, we present evaluations of its whole-body control performance, including locomotion. This is the first time to report a bipedal locomotion by an EHA driven humanoid. We first confirm that Hydra can realize a position feedback control with enough stiffness to realize a position control based locomotion. Secondly, we show that the joint backdrivability can suppress the effect of a disturbance applied to the distal part of the robot on the whole-body motion. As the result, we realized a torque control based locomotion with both a proper COM stabilization and nullspace compliance.**

I. Introduction

For the robots that perform tasks in uncertain environments such as daily life environments, small-scale factories with human workers, and disaster scenes, it is a critical requirement for their joints to have a high backdrivability. A difficulty of the actuators with highly geared motors or servovalve hydraulics, is their limited backdrivability, due to the high friction in the force transmission process. One approach is to measure the joint torque and actively realize the backdrivability [1]. To handle the limitation that impulsive disturbances exceeding their control bandwidth cannot be treated, Boaventura et al. [2] utilized a high bandwidth servovalve hydraulic system with the bandwidth of 250 Hz, regarding its high energy loss is affordable for the high performance. Instead of the active backdrivability on the non-backdrivable hardwares, actuators with an intrinsically backdrivable hardware structure have advantages in the efficiency, fail-safe property, and compliance in the wide frequency. The major approach is to insert a series elasticity between the non-backdrivable actuator and the joint, originating from the Recently, they are successfully integrated into humanoids such as the work by Tsagarakis et al. [3]. Another approach to realize mechanical backdrivability is to simply remove or reduce the high friction transmissions and increase the motor torque. This direct drive approach with the initial works by Asada et al. [4] has recently realized highly dynamic motions in the works by Wensing et al. [5].

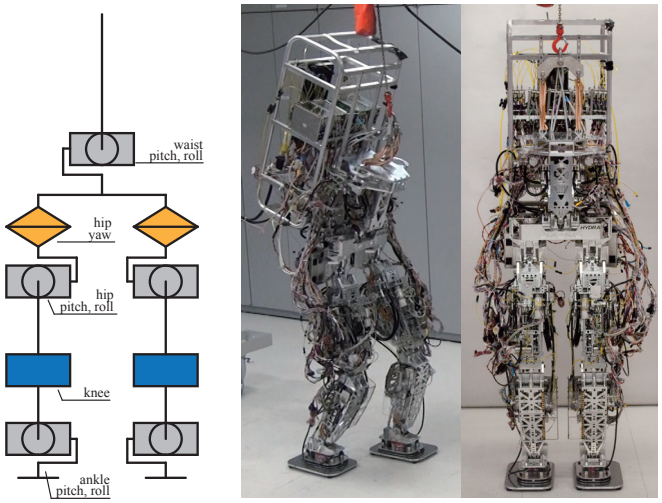

Fig. 1. Joint arrangement and outlook of the enlightened lower body model of Hydra. It has 14 EHA driven joints, weighting 74 kg.

For the series elastic actuators, their control bandwidth is limited by the low resonant frequency of the elastic element. For the direct drive approaches, the torque density which here we define as the torque to weight ratio, is limited to drive a large DoF robot such as a humanoid robot. Electro-Hydrostatic Actuator (EHA) is a closed circuit hydraulic system, where an actuator and a collocated pump are directly connected with a simple pipeline without regulation valves. Unlike open circuit systems such as servovalve hydraulics, each actuator is self-contained and independent from each other. The structure of an EHA driven robot, therefore, is close to the gear or ball screw driven robots, replacing the mechanical transmission to a hydrostatic one. EHA has advantages over open circuit hydraulic systems in the system simplicity, fail tolerance, and energy efficiency. The early works to apply EHA or HST (Hydrostatic Transmission) to robot joints include the work by Bobrow et al. [6] and Habibi et al. [7], and recently Alfayad et al. [8]. Besides those works, Kaminaga et al. [9] firstly focused on their possibility of high backdrivability and experimentally showed that with a proper low friction design, they can realize superior backdrivability than a gear driven joint.

* This work was supported by New Energy and Industrial Technology Development Organization (NEDO) The International R&D and Demonstration Project on Robotic Field / Research and Development of Disaster-Response Robot Open Platform (FY2014-FY2015), and NEDO Core Technology Development of Next- Generation Robots, Innovative Robot Element Technology, “Field Actuation Technology using Compact Hydraulic Actuators and Fuel Cell / Rechargeable Battery Hybrid Power Supply”.

[1]T. Ko, K. Yamamoto, K. Murotani and Y. Nakamura are with Graduate School of Information Science and Technology, The University of Tokyo, 7-3-1 Hongo, Bunkyo-Ku, Tokyo 113-8656, Japan. kang@ynl.t.u-tokyo.ac.jp

To realize a humanoid robot with intrinsically backdrivable but high control bandwidth joints, we developed the hydrostatically driven humanoid Hydra. While the overview of its mechanism [10]was reported in the literature, its high bandwidth property and backdrivability were not evaluated. In this paper, after an overview of Hydra and its actuator, we first present its high stiffness control performance, which is realized by the high joint control bandwidth. With the combination of a high gain joint position controller and the capture point tracking controller by Englsberger et al. [11], we realized the first example of the bipedal locomotion by an EHA driven robot. Secondly, we present its high compliance control, which is realized by the high joint backdrivability. As the result, we perform a locomotion that simultaneously realize the proper viscoelasticity of the COM and a high compliance in the nullspace.

II. Electro-Hydrostatic Actuators and the Hydrostatically Driven Humanoid Hydra

Electro-Hydrostatic Actuators are hydraulic systems with closed hydraulic circuits. In an EHA-driven system with multiple axes, each actuator unit has its own exclusive pump. The pumps are driven by electric motors and mostly placed close to the actuator. The control of the actuator, such as cylinder force or position, is achieved by controlling the discharging volume of the fluid out from the pump. This is done by changing the displacement of a constant-velocity pump, or changing the torque of the electric motor driving a fixed displacement pump. Here we treat the latter case. Servo-valve controlled hydraulic systems, which are commonly adopted for most of the hydraulic robots such as Atlas [12], HyQ [13], and CB [14], in contrast, have open hydraulic circuits. In a servovalve controlled hydraulic system, a central pump serves as the constant pressure source. Each actuator has its own servovalve, regulating the source pressure to the required value to control the actuator force or position. The advantages of a servovalve controlled system over an EHA-driven system are (1) high torque density and (2) high control bandwidth. The advantages of a EHA-driven system over a servovalve controlled system are (1) high energy efficiency and (2) intrinsic backdrivability.

An EHA can be also assumed as an actuator which replace the mechanical transmission of a geared motor by a hydrostatic transmission. The removal of the gear meshing parts can reduce the mechanical contact friction, therefore a high backdrivability can be achieved without relying on a series elasticity. It also achieves high mechanical reliability and impact resistance. The disadvantage of EHA compared with the geared motors are the heavier weight, complex system, and lower torque efficiency due to the internal leakage and viscous friction.

To attain enough torque density for a legged robot, the key is how to control the internal leakage [15]. While the amount of the leakage depends on the cube of the internal gap, we found that our lightweight EHA with aluminum material resulted in an unexpected internal gap due to the internal pressure and a careful design with high stiffness components can drastically reduce the leakage [16]. The heat problem was also unavoidable, since the internal leakage results higher fluid temperature therefore lower viscosity and even more internal leakage. To effectively cool the closed hydraulic circuit, we directly merged the water cooling circuit into the pump casing. On the actuator side, the low internal leakage property cannot prevent the low friction property to maintain the high backdrivability. To reduce the friction due to the oil seal, we developed a double rod cylinder with beam structure, whose prototype is described in [17]. In this actuator, the piston rod diameter is minimized since the beam structure supports both ends of the piston rod and prevents buckling. The resulted linear EHA has 1.2 kg weight including the 200 W motor, and can output 1500 N force with 50 mm stroke. Table I summarizes its specification.

TABLE I
Specification of the lightweight linear EHA to drive Hydra.

Thrust Force	1500 N
Maximum Speed	0.2 m/s
Piston Stroke	50 mm
Pressure Control Bandwidth[2]	100 Hz
Transfer Pressure	5.3 MPa
Motor Power	200 W
Equivalent Leadscrew Pitch[3]	1.5 mm/rev

Hydra has 40 DoF driven by EHA – 22 of them are driven by the linear EHA mentioned above, 8 of them driven by rotary vane motor type EHA, and 10 DoF are for the hands driven by two five-DoF cluster EHA. The total weight is around 130 kg with 180 cm height. In this paper, we removed the arms for the ease of maintenance and experiments. In that case the total weight is around 74 kg with 14 DoF. The outlook of the enlightened version of Hydra is shown in Figure 1. All of the joints are torque controllable with the pressure sensors on the actuator. The actuator force can be also measured through a strain gauge attached on the connecting rod. In this work, the force measurement by the strain gauge was not enabled, while we found that there was no delay between the two. The joint position is acquired through the linear encoder on the actuator. Two 6-axis force torque sensor is attached on the foot to measure the ground reaction force. The control system has three layers, handling the motor current feedback in 20 kHz on FPGAs, pressure control in 5 kHz on microcontrollers, and whole-body control in 1 kHz [18].

III. Stiff Motion Realized by the High Bandwidth

Joint position control based walking frameworks are widely studied for the position controlled robots since they are robust against joint torque error and mass parameters error. While Hydra is a torque control based robot, it needs

[2]Under the condition that the piston is fixed at the end of the cylinder.

[3]Since the linear EHA converts the rotary input to a linear output, the effective reduction ratio can be described as the pitch of a leadscrew. This is the ideal value when the internal leakage is ignored.

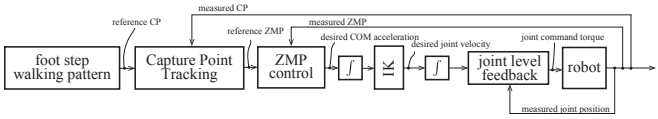

Fig. 2. Block diagram of Hydra's position-control based walking controller based on the Capture Point Tracking control [11].

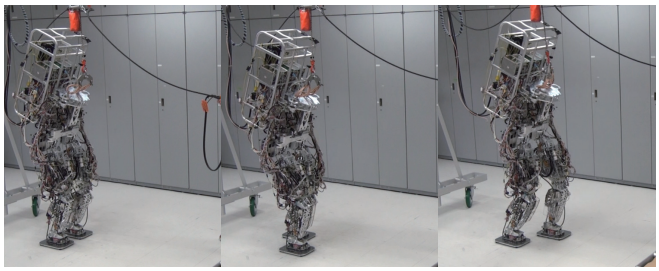

Fig. 3. Outlook of the walking experiment based on the Capture Point Tracking control. The robot could successfully conduct the walking motion with 20 cm stride and 30 mm step height. The step time was set as 1 second.

the capability to support those control framework as a robot platform. In this section, we construct an independent joint level position feedback controller on the local torque controller and treat Hydra as a position control based robot, therefore evaluate its locomotion performance based on the position control. As the whole-body controller, we implemented the Capture Point Tracking controller by Englsberger et al. [11].

Figure 2 shows the structure of the controller. From the predefined footstep, the reference Capture Point (CP) trajectory can be preplanned. The CP tracking controller compares the current CP and the reference CP trajectory therefore output the desired ZMP. The desired COM acceleration is then generated to fulfill the desired ZMP. The desired COM velocity, which is integrated from the desired acceleration, is projected to the desired joint velocity, with the task priority in addition to the other tasks such as moving leg path and body attitude. Finally, the desired joint velocity is integrated as the command joint position and sent to the joint level position controller.

Figure 3 shows the view of the walking experiment. The robot could successfully conduct the walking motion with 20 cm stride and 30 mm step height. The step time was set as 1 second. The time transition of the desired/measured CP and desired/measured ZMP is shown in Figure 4. The actual CP varies earlier than the command one since the controller tries to follow the dT time future point. In this case dT is set as 0.2 second. The command ZMP is noisy due to the noisy measure CP, originated from the noisy estimated COM velocity. The actual ZMP is smooth, since the integration and conversion from the COM acceleration to the joint command position plays the role of a low-pass filter. The actual ZMP follows the command one with 47 mm RMS error.

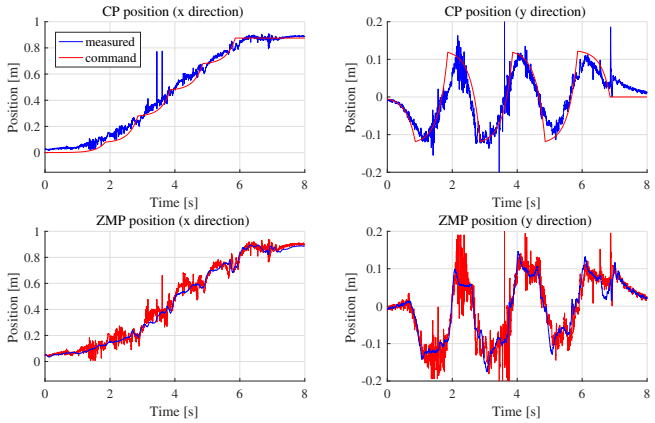

Fig. 4. Time transition of the command/measured CP and command/measured ZMP during the walking experiment.The actual CP varies earlier than the command one since the controller tries to follow the dT time future point. In this case dT is set as 0.2 second. The command ZMP is noisy due to the noisy measure CP, originated from the noisy estimated COM velocity. The actual ZMP is smooth, since the integration and conversion from the COM acceleration to the joint command position plays the role of a low-pass filter. The actual ZMP follows the command one with 47 mm RMS error.

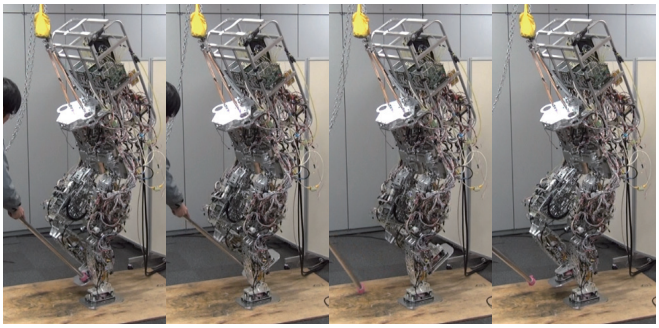

Fig. 5. Experiment to examine the disturbance rejection performance of the backdrivable joints. The robot is standing by the left leg and a disturbance is manually applied on the right foot. The robot is under a joint level position control, without whole-body feedback. Two experiments were conducted: one with high joint stiffness and another with low joint feedback gain on the right leg therefore it can absorb disturbance.

IV. Compliant Motion Realized by the Backdrivability

A. Disturbance Rejection with Backdrivability

An advantage of robots with backdrivable joints it that if an external force is applied to the distal parts of the body, the local joints can absorb it without harming the overall locomotion. In other words, even if the robot is disturbed in the configuration space, it should not react on it as long as the tasks in the operational space such as COM motion is not disturbed. This is difficult for the position control based robot, which has high gain configuration space level position feedback. To evaluate the disturbance rejection performance of Hydra, we first conducted an experiment shown in Figure 5. The robot was standing by the left leg and a disturbance was manually applied on the right foot. The robot was under a joint level position control, without

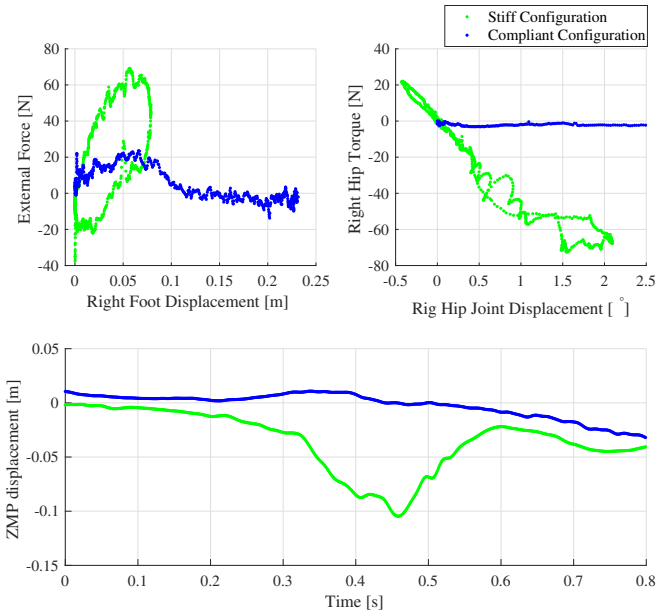

Fig. 6. Displacement against the disturbance in the operational space and configuration space, and variation of ZMP during the initial 0.8 second after the disturbance happens. The green makers show the case with high gain (stiff configuration) and the blue markers show the case with the low gain (compliant configuration). On the top left is the right foot displacement against the force in the x (sagittal) direction. On the top right is the relationship between the joint angle displacement and joint torque of the right hip pitch joint. On the bottom of the figure, the time transition of the ZMP on the left foot is shown. The displacement represents the distance between the current ZMP position and the initial position.

the whole-body feedback. Two experiments were conducted: one with high joint stiffness and another with low joint feedback gain on the right leg therefore it can absorb the disturbance by the local joints. The figure shows the one with the compliant configuration. With the disturbance, the right leg moved rapidly and the external force was absorbed as the acceleration of the right leg. The rest of the body therefore did not receive an impulsive effect and the robot could keep standing.

In Figure 6, the values of the initial 0.8 second after the disturbance is shown. On the top left is the right foot displacement against the force in the x (sagittal) direction. The displacement is calculated from the joint angles and forward kinematics. The force is measured by the foot force sensor on the right foot, which is not used in the control in this experiment. The green makers show the case with high gain (stiff configuration) and the blue markers show the case with the low gain (compliant configuration). While the stiff case showed a high operational space impedance, in the compliant case it was largely reduced. The relatively high impedance at the beginning of the compliant case is due to the acceleration of the foot, since the impedance cannot be seen when the displacement is large. On the top right is the relationship between the joint angle displacement and joint torque of the right hip pitch joint. This graph shows that the disturbance force is not transferred to the COM, thanks to the high joint backdrivability. This results in slower disturbance on the ZMP. On the bottom of the figure, the time transition of the ZMP on the left foot is shown. Unlike the stiff case where it varies rapidly, in the compliant case the velocity was suppressed to around 30% value.

B. Coexistence of a Proper COM Stabilization and Nullspace Compliance

To keep the balance of a torque controlled robot, instead of to explicitly consider the ground reaction force, a proper setting of COM viscoelasticity in the task space is also a solution [19]. The advantage of this approach is that the COM viscoelasticity can be projected to the joint space one, and the feedback loop can be closed in the joint level. This allows to realize a whole-body compliant motion with the same controller structure with the position control based controller. The projection of the taskspace viscoelasticity to the joint space one is realized by the Resolved Viscoelasticity Control (RVC) [19]. The joint viscoelasticity and task viscoelasticity can be written as follows:

$$\boldsymbol{\tau} =^{ref} \boldsymbol{\tau} + \boldsymbol{K}_\theta({}^{ref}\boldsymbol{\theta} - \boldsymbol{\theta}) + \boldsymbol{D}_\theta({}^{ref}\dot{\boldsymbol{\theta}} - \dot{\boldsymbol{\theta}}) \quad (1)$$

$$\boldsymbol{f}_i =^{ref} \boldsymbol{f}_i + \boldsymbol{K}_i({}^{ref}\boldsymbol{p}_i - \boldsymbol{p}_i) + \boldsymbol{D}_i({}^{ref}\dot{\boldsymbol{p}}_i - \dot{\boldsymbol{p}}_i) \quad (2)$$

where $\boldsymbol{\theta}, \boldsymbol{\tau} \in \mathbb{R}^n$ denotes joint position and torque, ${}^{ref}*$ is the referenece value of $*$, $\boldsymbol{p}_i, \boldsymbol{f}_i \in \mathbb{R}^3$ denotes a feature quantity in the task space such as COM position and the force acting on it, and $\boldsymbol{K}_\theta, \boldsymbol{D}_\theta \in \mathbb{R}^{n\times n}$, $\boldsymbol{K}_i, \boldsymbol{D}_i \in \mathbb{R}^{3\times 3}$ denotes the viscoelasticity in the configuration space and task space. For the simplicity, we focus on the compliance, which is the inverse of stiffness $\boldsymbol{C}_i = \boldsymbol{K}_i^{-1}, \boldsymbol{C}_\theta = \boldsymbol{K}_\theta^{-1}$. Their relationship is given as:

$$\boldsymbol{C}_i = \boldsymbol{J}_i \boldsymbol{C}_\theta \boldsymbol{J}_i^T \quad (3)$$

where $\boldsymbol{J}_i \in \mathbb{R}^{3\times n}$ is the Jacobian matrix for the task $\boldsymbol{p}_i$.

With redundant DoF, Eq. 3 is solved as

$$\boldsymbol{C}_\theta = \boldsymbol{J}_i^{\#} \boldsymbol{C}_i \boldsymbol{J}_i^{\#T} + ({}^d\boldsymbol{C}_\theta - \boldsymbol{J}_i^{\#} \boldsymbol{J}_i \, {}^d\boldsymbol{C}_\theta \boldsymbol{J}_i^T \boldsymbol{J}_i^{\#T}) \quad (4)$$

where $\boldsymbol{J}_i^{\#}$ is the pseudo-inverse of $\boldsymbol{J}_i$ and ${}^d\boldsymbol{C}_\theta \in \mathbb{R}^n$ is an arbitrary desired joint compliance[19]. The desired joint compliance ${}^d\boldsymbol{C}_\theta$ is fulfilled by $\boldsymbol{C}_\theta$ with a least square error under the condition that Eq. 3 is fulfilled. Setting ${}^d\boldsymbol{C}_\theta$ as a high value, we can realize highly compliant motion in the direction that the task is not affected.

For balancing or locomotion, two approaches are possible for the task space or the COM viscoelasticity. One is to make $\boldsymbol{K}_i$ as stiff as possible and change the target COM position according to the ground reaction force. It results in a simpler controller, however, if we can adjust $\boldsymbol{K}_i$ to a proper value that realize the same property of the former case. In fact, it is shown in the literature [19] that the COM viscoelasticity can be identically converted from the PD gain of a linear feedback controller manipulating the ZMP to maintain the COM position. When the control law is given as:

$$\boldsymbol{u} =^{ref} \boldsymbol{u} + \boldsymbol{F}({}^{ref}\boldsymbol{x} - \boldsymbol{x}) \quad (5)$$

where $\boldsymbol{u} = [x_z \; y_z]^T$ is the position of ZMP, $\boldsymbol{F} = [\boldsymbol{F}_k \; \boldsymbol{F}_d]$ is the state feedback gain, $\boldsymbol{x} = [x_G \; y_G \; \dot{x}_G \; \dot{y}_G]^T$ is the

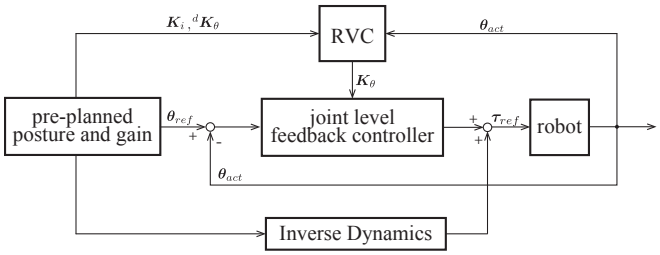

Fig. 7. Block diagram of hydra's resolved viscoelasticity controller. The RVC module updates the gain matrix, according to the current joint position. The joint position feedback controller receives the gain matrix and conduct position control. Since the joint gain matrix is not diagonal, this feedback is done as the whole body and the resulted whole body torque is sent to the robot. To achieve dynamic motions with low feedback gain, feed forward torque calculated from the inverse dynamics plays an important role.

robot state containing the COM position and velocity, the equivalent COM viscoelasticity $\boldsymbol{K}_G, \boldsymbol{D}_G$ is given as:

$$\boldsymbol{K}_G = \begin{bmatrix} -m\omega^2(\boldsymbol{E}+\boldsymbol{F}_k) & \boldsymbol{0} \\ \boldsymbol{0} & k_z \end{bmatrix} \quad (6)$$

$$\boldsymbol{D}_G = \begin{bmatrix} -m\omega^2\boldsymbol{F}_d & \boldsymbol{0} \\ \boldsymbol{0} & d_z \end{bmatrix} \quad (7)$$

where $\boldsymbol{E}$ is identity matrix, m is the weight of the robot, and $\omega = \sqrt{g/z}$ with g, z denoting the acceleration of gravity and height of the COM. In the vertical direction, a proper PD gain k_z, d_z is set. For the detailed theory of RVC and its preliminary experiments on Hydra, see [20].

Figure 7 shows the structure of the RVC controller. In addition to the footstep, the joint trajectory is also pre-planned. The RVC module updates the joint stiffness, in other words the gain matrix, according to the current joint position. The joint position feedback controller receives the gain matrix and conduct position control. Since the joint gain matrix is not diagonal, this feedback is done as the whole body and the resulted whole body torque is sent to the robot. To achieve dynamic motions with low feedback gain, feed forward torque calculated from the inverse dynamics plays an important role. The controller shown in Figure 7 is much simpler than the one in 2. This is because the RVC framework does not have an explicit ground force feedback with the CP and ZMP. Instead, the force feedback is implicitly conducted by the joint torque feedback.

A practical advantage of the RVC is that since the task space feedback is not directly done in the task space but realized through the projected joint level feedback, we can explicitly examine the gain matrix. Even though the EHA developed for Hydra has an enhanced response property, the control bandwidth is still limited. This leads the limitation of the task space level or joint level feedback gain. While the output joint gain matrix from the RVC is not diagonal, the diagonal elements still have a relatively dominant value. Comparing it with the fine-tuned gains for the individual joints, we can roughly estimate whether the task space feedback gain is affordable for the real hardware. This is a strong tool since the multiple task space gains such as

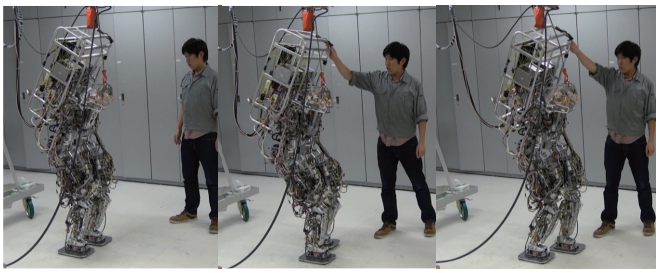

Fig. 8. Outlook of the walking experiment based on the resolved viscoelasticity control. During the walking it kept compliant in the nullspace therefore even though a disturbance force was manually applied on the top of the backpack, its effect on the locomotion was suppressed by the compliant motion of the waist joints.

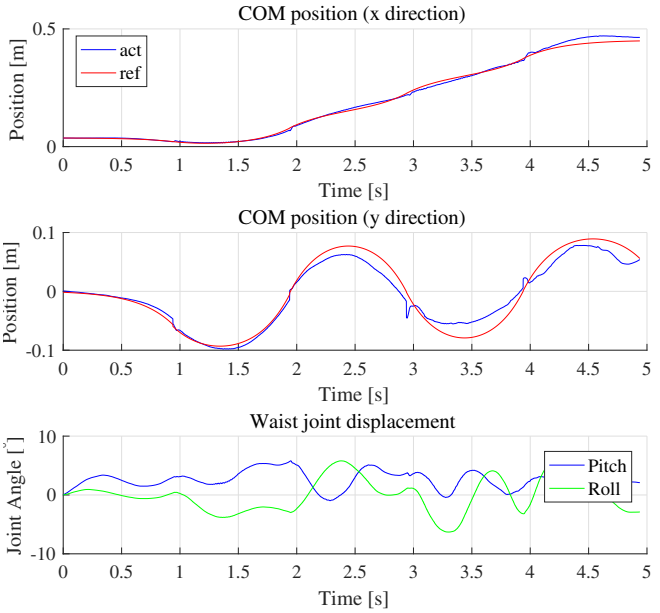

Fig. 9. Time transition of the command/actual COM position and the joint displacement of the waist joint. A large disturbance was applied on the top of the backpack when the time was 2 - 2.5 second. The bottom graph shows that the waist joint largely moved according to the disturbance. From the COM trajectory, however, it is difficult to see its effect. This shows that the controller successfully separated the motion of the COM and nullspace and absorbed the disturbance by the nullspace compliance.

COM, moving leg or body attitude result in a large DoF of gain tuning, which requires numerous try and error.

Figure 8 shows the view of the dynamic walking experiment based on the RVC. During the walking it kept compliant in the nullspace therefore even though a disturbance force was manually applied on the top of the backpack, its effect on the locomotion was suppressed by the compliant motion of the waist joints. Figure 9 shows the time transition of the command/actual COM position (estimated from the forward kinematics from the joint angles) and the joint displacement of the waist joint. Unlike the case with the position control based walking, no CP or ZMP information is used in the control therefore it is now shown in the graph. The command COM position, on the other hand, is available from the preplanned joint trajectory. A large disturbance was applied

on the top of the backpack when the time was 2 - 2.5 second. The bottom graph shows that the waist joint largely moved according to the disturbance. From the COM trajectory, however, it is difficult to see its effect. This shows that the controller successfully separated the motion of the COM and nullspace and absorbed the disturbance by the nullspace compliance.

V. Discussion

The compliant motion realized in this work proved the concept of EHA as an intrinsically backdrivable robot actuator. The remaining limitation is the torque density of the actuator. With the analysis on the internal leakage which decreases the energy transfer efficiency of the transmission, we improved the torque density of our developed EHA to have a superior torque performance compared with other works on the small-sized EHA. Nevertheless, it is still limited compared with servovalve-controlled hydraulics or geared motors. For example, the maximum force 1500 N of our EHA is still smaller compared with the 5329/4420 N force realized by Hyon et al. [21] for their biped robot. For the current stage, addition of a heavy upper body will cause a large limitation on its locomotion performance. While currently we treat this lack of torque as a tradeoff to acquire the intrinsic backdrivability, we are now working on an EHA with a larger torque [22], based on the experience acquired in this work.

VI. Conclusion

In this paper, we presented the stiff control and compliant control performance of the hydrostatically driven humanoid Hydra. The conclusion is as follows:

1) With the stiff control realized by the high actuator control bandwidth, we performed the first example of the bipedal locomotion by an EHA driven robot, which was a 20 cm stride and 1 second step time walk.
2) With its high joint backdrivability, Hydra can prevent a disturbance force applied on a distal link to be transferred to other links. By simply reducing the position feedback gain, the effect of a disturbance force on ZMP variation was suppressed to 30%.
3) We performed a torque control based locomotion that simultaneously realize the proper viscoelasticity of the COM and nullspace compliance.

Acknowledgment

The authors wish to thank Dr. Hiroshi Kaminaga, Satoshi Yorita, Shunsuke Sato, Ryo Masumura, and Mitsuo Komagata for the collaboration in the initial development of Hydra.

References

[1] J. Englsberger, A. Werner, C. Ott, B. Henze, M. A. Roa, G. Garofalo, R. Burger, A. Beyer, O. Eiberger, K. Schmid, *et al.*, "Overview of the torque-controlled humanoid robot toro," in *IEEE-RAS Int'l Conf. on Humanoid Robots*, 2014, pp. 916–923.

[2] T. Boaventura, J. Buchli, C. Semini, and D. G. Caldwell, "Model-based hydraulic impedance control for dynamic robots," *IEEE Transactions on Robotics*, vol. 31, no. 6, pp. 1324–1336, 2015.

[3] N. G. Tsagarakis, D. G. Caldwell, F. Negrello, W. Choi, L. Baccelliere, V. Loc, J. Noorden, L. Muratore, A. Margan, A. Cardellino, *et al.*, "Walk-man: A high-performance humanoid platform for realistic environments," *Journal of Field Robotics*, vol. 34, no. 7, pp. 1225–1259, 2017.

[4] H. Asada and T. Kanade, "Design concept of direct-drive manipulators using rare-earth DC torque motors," in *Proc. of the Int'l Joint Conf. on Artificial intelligence*, 1981, pp. 775–778.

[5] P. M. Wensing, A. Wang, S. Seok, D. Otten, J. Lang, and S. Kim, "Proprioceptive Actuator Design in the MIT Cheetah: Impact Mitigation and High-Bandwidth Physical Interaction for Dynamic Legged Robots," *IEEE Transactions on Robotics*, vol. 33, no. 3, pp. 509–522, 2017.

[6] J. E. Bobrow and J. Desai, "A high torque to weight ratio robot actuator," *Robotica*, vol. 13, no. 2, pp. 201–208, 1995.

[7] S. Habibi and A. Goldenberg, "Design of a new high performance electrohydraulic actuator," in *Proc. of IEEE/ASME International Conference on Advanced Intelligent Mechatronics*. IEEE, 1999, pp. 227–232.

[8] S. Alfayad, F. B. Ouezdou, F. Namoun, and G. Gheng, "High performance integrated electro-hydraulic actuator for robotics–Part I: Principle, prototype design and first experiments," *Sensors and Actuators A: Physical*, vol. 169, no. 1, pp. 115–123, 2011.

[9] H. Kaminaga, T. Yamamoto, J. Ono, and Y. Nakamura, "Backdrivable miniature hydrostatic transmission for actuation of anthropomorphic robot hands," in *Proc. of IEEE-RAS Int'l Conf. on Humanoid Robots*, 2007, pp. 36 –41.

[10] H. Kaminaga, T. Ko, R. Masumura, M. Komagata, S. Sato, S. Yorita, and Y. Nakamura, "Mechanism and Control of Whole-Body Electro-Hydrostatic Actuator Driven Humanoid Robot Hydra," in *International Symposium on Experimental Robotics*. Springer, 2016, pp. 656–665.

[11] J. Englsberger, C. Ott, M. Roa, A. Albu-Schäffer, and G. Hirzinger, "Bipedal walking control based on capture point dynamics," in *IEEE/RSJ International Conference on Intelligent Robots and Systems*. IEEE, 2011, pp. 4420–4427.

[12] "Boston dynamics: Atlas - the agile anthropomorphic robot," *http://www.bostondynamics.com/robot_Atlas.html*.

[13] C. Semini, N. G. Tsagarakis, E. Guglielmino, M. Focchi, F. Cannella, and D. G. Caldwell, "Design of hyq–a hydraulically and electrically actuated quadruped robot," *Proc. of the Institution of Mechanical Engineers, Part I: Journal of Systems and Control Engineering*, vol. 225, no. 6, pp. 831–849, 2011.

[14] G. Cheng, S.-H. Hyon, J. Morimoto, A. Ude, J. G. Hale, G. Colvin, W. Scroggin, and S. C. Jacobsen, "Cb: A humanoid research platform for exploring neuroscience," *Advanced Robotics*, vol. 21, no. 10, pp. 1097–1114, 2007.

[15] T. Ko, H. Kaminaga, and Y. Nakamura, "Key Design Parameters of a Few Types of Electro-Hydrostatic Actuators for Humanoid Robots," in *Advanced Robotics*, (under review).

[16] ——, "Underactuated four-fingered hand with five electro hydrostatic actuators in cluster," in *Proc. of IEEE Int'l Conf. on Robotics and Automation*, 2017, pp. 620–625.

[17] H. Kaminaga, S. Otsuki, and Y. Nakamura, "Development of High-Power and Backdrivable Linear Electro-Hydrostatic Actuator," in *Proc. of IEEE-RAS Int'l Conf. on Humanoid Robots*, 2014, pp. 973–978.

[18] T. Ko, H. Kaminaga, and Y. Nakamura, "Current-Pressure-Position Triple-Loop Feedback Control of Electro-Hydrostatic Actuators for Humanoid Robots," in *Advanced Robotics*, (under review).

[19] K. Yamamoto, "Resolved multiple viscoelasticity control for a humanoid," *IEEE Robotics and Automation Letters*, vol. 3, no. 1, pp. 44–51, 2018.

[20] K. Yamamoto, T. Ko, K. Murotani, and Y. Nakamura, "Experimental Validation of Resolved Viscoelasticity Control on Hydrostatically driven Humanoid Hydra," in *International Symposium on Experimental Robotics*. Springer, 2018 (accepted).

[21] S. H. Hyon, D. Suewaka, Y. Torii, and N. Oku, "Design and Experimental Evaluation of a Fast Torque-Controlled Hydraulic Humanoid Robot," *IEEE/ASME Transactions on Mechatronics*, vol. 22, no. 2, pp. 623–634, 2017.

[22] M. Komagata, T. Ko, and Y. Nakamura, "Small Size Hydraulic Pumps with Low Heat Generation for Electro Hydrostatic Actuation of Humanoid Robots," in *Proc. of IEEE-RAS Int'l Conf. on Humanoid Robots*, 2018 (Accepted).